Dynamics of Solar and Stellar Convection Zones and Atmospheres
Proceedings IAU Symposium No. 365 No. ,
Alexander Getling & Leonid Kitchatinov, eds.
doi:10.1017/xxxxx

Effects of rotation and surface forcing on deep stellar convection zones

Petri J. Käpylä

Leibniz-Insitute for Solar Physics (KIS), Schöneckstraße 6, 79104 Freiburg im Breisgau, Germany

Abstract. The canonical undestanding of stellar convection has recently been put under doubt due to helioseismic results and global 3D convection simulations. This "convective conundrum" is manifested by much higher velocity amplitudes in simulations at large scales in comparison to helioseismic results, and the difficulty in reproducing the solar differential rotation and dynamo with global 3D simulations. Here some aspects of this conundrum are discussed from the viewpoint of hydrodynamic Cartesian 3D simulations targeted at testing the rotational influence and surface forcing on deep convection. More specifically, the dominant scale of convection and the depths of the convection zone and the weakly subadiabatic – yet convecting – Deardorff zone are discussed in detail.

Keywords. Convection, turbulence, Sun: rotation, Sun: interior

1. Introduction

The solar convective envelope rotates differentially, such that the rotation rate at the equator is about 40 per cent faster than at near the poles. Furthermore, helioseismology has revealed that the angular velocity Ω increases (decreases) with radius near the equator (high latitudes), with narrow shear layers at the base and near the surface of the convection zone (e.g. Thompson et al. 2003). This large-scale phenomenon is one of the principal observations that global 3D simulations seek to reproduce. Early 3D simulations of the late 1970s and early 1980s were able to capture this (e.g. Gilman 1977), although dynamo cycles in those simulations did not match that of the Sun (e.g. Gilman 1983; Glatzmaier 1985). However, it took another two decades for such simulations to become more mainstream (e.g. Brun et al. 2004; Ghizaru et al. 2010; Brown et al. 2011; Käpylä et al. 2012); see also Käpylä et al. (2023) for a recent review. Soon thereafter it was realized that obtaining solar-like differential rotation (fast equator, slow poles) with simulations with the nominal solar rotation rate and luminosity is highly non-trivial (e.g. Gastine et al. 2014; Käpylä et al. 2014; Fan and Fang 2014; O'Mara et al. 2016). This is thought to be due to too weak rotational influence on the dominant convective scales, or equivalently, a too low Coriolis (inverse Rossby) number.

At the same time, efforts were made to study the velocity amplitudes in the Sun using helioseismology (Hanasoge et al. 2010, 2012). These studies led to the realization that convective amplitudes at horizontal scales of the order of hundreds of Mm in the Sun appear to be several orders of magnitude weaker than in the global simulations, and that the velocity power spectrum in the Sun peaks at supergranular scale of 20-30 Mm. While the difference between helioseismic and simulation results has reduced somewhat in the meantime, a large discrepancy remains (e.g. Proxauf 2021). Adding to the puzzle are the results of Greer et al. (2015) from a ring-diagram analysis that shows high velocity amplitudes in the near-surface shear layer of the Sun consistent with global 3D convection simulations.

Several physical processes have been suggested as possible solutions of the convective conundrum. Rotationally constrained convection in the deep parts of the convection zone is one such possibility (Featherstone and Hindman 2016; Vasil et al. 2021). Linear stability analysis and non-linear simulations of convection indicate that the convective scale decreases with

rotation. Given that the velocity power spectrum peaks at the supergranular scale in the Sun, it is has been conjectured that this scale coincides with the largest convectively driven scale in the deep convection zone. The question if convection in the Sun is indeed sufficiently constrained by rotation was studied systematically in Käpylä (2023a). These results are reviewed in more detail below.

Another possibility is that the solar convection zone is in fact largely subadiabatic, that is, the thermal stratification is formally weakly Schwarzschild stable. This can be enabled by plumes originating near the surface that transport cool low entropy material deep into the interior far beyond the formally unstable layer. This is related to the idea that convection in the Sun is driven by the cooling at the surface rather than by a superadiabatic temperature gradient throughout the convection zone (Stein and Nordlund 1989; Spruit 1997). Such non-local driving of convection due to surface cooling has been dubbed "entropy rain" (e.g. Brandenburg 2016). The convective flux in the stably stratified, but convecting, layer is carried by a counter-gradient term proportional to the variance of entropy fluctuations (Deardorff 1961, 1966). Hence this layer is referred to as the Deardorff zone. Simulations of overshooting convection routinely capture such subadiabatic layers if the transition between the radiative and convective regions is smooth enough (e.g. Roxburgh and Simmons 1993; Tremblay et al. 2015; Käpylä et al. 2017; Hotta 2017). Most of the previous works considered non-rotating cases, whereas here recent results of Käpylä (2023a), where the effects of rotation were included, are discussed.

Finally, the strength of the surface forcing depends on the physics near the surface of the star. In real stellar convection zones the density drops vertigineously near the surface and this cannot be directly reproduced in numerical simulations (e.g. Kupka and Muthsam 2017; Käpylä et al. 2023). Here preliminary results from an effort to study the effects of surface forcing by varying the (imposed) superadiabatic temperature gradient at the surface are discussed based on earlier models presented in Käpylä et al. (2017). The novelty of these simulations is that they are constructed in such a way that the depth and structure of the convection zone are self-consistent results of the models instead of being fixed from the outset.

2. The model

The set-up is the same as in Käpylä (2019), Käpylä (2021), and Käpylä (2023a), and the PENCIL CODE (Pencil Code Collaboration et al. 2021) was used to make the simulations. The simulation domain is a rectangular box with dimensions $(L_x, L_y, L_z) = (4, 4, 1.5)d$, where d is the depth of the initially isentropic layer which is situated between $0 \le z/d \le 1$. Initially this layer is sandwiched between a radiative layer with polytropic index $n = 3.25$ ($-0.45 \le z/d < 0$) and an isothermal layer ($1 < z/d \le 1.05$). The equations for compressible hydrodynamics are solved:

$$\frac{D\ln\rho}{Dt} = -\boldsymbol{\nabla}\cdot\boldsymbol{u}, \tag{1}$$

$$\frac{D\boldsymbol{u}}{Dt} = \boldsymbol{g} - \frac{1}{\rho}(\boldsymbol{\nabla}p - \boldsymbol{\nabla}\cdot 2\nu\rho\mathsf{S}) - 2\boldsymbol{\Omega}\times\boldsymbol{u}, \tag{2}$$

$$T\frac{Ds}{Dt} = -\frac{1}{\rho}\left[\boldsymbol{\nabla}\cdot(\boldsymbol{F}_{\rm rad}+\boldsymbol{F}_{\rm SGS}) - \mathscr{C}\right] + 2\nu\mathsf{S}^2, \tag{3}$$

where $D/Dt = \partial/\partial t + \boldsymbol{u}\cdot\boldsymbol{\nabla}$ is the advective derivative, ρ is the density, $\boldsymbol{u}$ is the velocity, $\boldsymbol{g} = -g\hat{\boldsymbol{e}}_z$ with $g > 0$ is the acceleration due to gravity where $\hat{\boldsymbol{e}}_z$ is the unit vector along the vertical (z) direction, p is the gas pressure, ν is the viscosity, S is the traceless rate-of-strain tensor, $\boldsymbol{\Omega} = \Omega\hat{\boldsymbol{e}}_z$ is the rotation vector, T is the temperature, and s is the specific entropy. $\boldsymbol{F}_{\rm rad} = -K\boldsymbol{\nabla}T$ is the radiative flux where $K = K_0\rho^{-2}T^{6.5}$ is the heat conductivity following Kramers opacity law, and $\boldsymbol{F}_{\rm SGS} = -\chi_{\rm SGS}\rho T\boldsymbol{\nabla}s'$ is the subgrid-scale (SGS) entropy flux, where $\chi_{\rm SGS}$ is a constant SGS diffusivity and $s' = s - \bar{s}$ is the deviation of the entropy from its horizontally

averaged profile which is denoted by the overbar. The gas obeys the ideal gas equation $p = \mathscr{R}\rho T$, where $\mathscr{R} = c_P - c_V$ is the gas constant and where c_P and c_V are the specific heats in constant pressure and volume, respectively. Finally, $\mathscr{C}$ describes cooling near the surface.

In Käpylä (2023a) it was shown that a Coriolis number based on a hypothetical velocity $u_\star = (F_{\rm tot}/\rho)^{1/3}$ is equivalent to

$$\mathrm{Co_F} = 2\Omega H_{\rm p}\left(\frac{\rho}{F_{\rm tot}}\right)^{1/3} = (\mathrm{Ra_F^\star})^{-1/3}, \tag{4}$$

where $F_{\rm tot}$ is the total energy flux, $H_{\rm p} = (\mathrm{d}\ln\overline{p}/\mathrm{d}z)^{-1}$ is the pressure scale height, and

$$\mathrm{Ra_F^\star} = \frac{gF_{\rm tot}}{8c_P\rho T\Omega^3 H^2} = \frac{F_{\rm tot}}{8\rho\Omega^3 H_{\rm p}^3}, \tag{5}$$

is the flux-based diffusion-free modified Rayleigh number (e.g. Christensen 2002), where the length scale H was chosen such that $H = c_P T/g = H_{\rm p}$, where $H_{\rm p}$ is taken at the base of the convection zone. The advantage of $\mathrm{Co_F}$ is that it does not depend on any dynamical velocity or length scale and it can be computed using observables $(\Omega, F_{\rm tot})$ and quantities from stellar structure models $(\rho, H_{\rm p})$; see also the discussion in Käpylä (2023b). Further system parameters include the Taylor number $\mathrm{Ta} = 4\Omega^2 d^4/\nu^2$, and the Prandtl number related to the SGS diffusivity $\mathrm{Pr_{SGS}} = \nu/\chi_{\rm SGS}$. The energy flux is measured by the dimensionless flux $\mathscr{F}_{\rm n} = F_{\rm tot}/\rho c_{\rm s}^3$ at $z/d = -0.45$ in the initial non-convecting state. Diagnostic quantities include the Reynolds ($\mathrm{Re} = u_{\rm rms}/\nu k_1$) and Péclet number ($\mathrm{Pe} = u_{\rm rms}/\chi_{\rm SGS}k_1 = \mathrm{Pr_{SGS}Re}$), and the global Coriolis number $\mathrm{Co} = 2\Omega/(u_{\rm rms}k_1)$, where $u_{\rm rms}$ is the volume-averaged rms-velocity, and $k_1 = 2\pi/d$ is an estimate of the scale of the largest eddies. A more detailed description of the model is given in Käpylä (2023a).

Three main sets of runs (Sets A, B, and C) were made where Co was varied between 0 and about 17. The imposed flux $\mathscr{F}_{\rm n}$ was varied between the sets to study the scaling of dynamical quantities with respect to it. The diffusivities were varied proportional to $\mathscr{F}_{\rm n}^{1/3}$ to achieve the same Re, Pe, and Co in each set (cf. Käpylä et al. 2020, for more details). The primary difference between the sets is that the Mach number $\mathrm{Ma} = u_{\rm rms}/c_{\rm s}$, where $c_{\rm s}$ is the sound speed, and therefore relative stability of the radiative layer below the convection zone vary. In Sets A to C, $\mathrm{Re} = \mathrm{Pe} \approx 30\ldots40$ and $\mathrm{Pr_{SGS}} = 1$. A subset of Set A, denoted as Set Am, was repeated at a higher resolution (576^3 instead of 288^3 grid points), and correspondingly higher values of Reynolds and Péclet numbers ($\mathrm{Re} = \mathrm{Pe} \approx 65\ldots84$), while keeping $\mathrm{Ra_F^\star}$ fixed.

3. Rotational scaling of convection

In Käpylä (2023a) the scaling of various quantities in rotating convection were studied. The numerical results were compared with scalings derived for slow rotation where a balance between inertial and buoyancy forces is assumed and for rapid rotation where a balance between Coriolis, inertial, and Archimedean (buoyancy) forces, or the CIA balance (e.g. Stevenson 1979; Barker et al. 2014; Aurnou et al. 2020), is assumed. For the dominant convective scale this leads to:

$$\ell_{\rm conv} \sim H_{\rm p}\ \text{(slow rotation)},\quad \text{and}\quad \ell_{\rm conv} \sim H_{\rm p}\mathrm{Co}^{-1/2}\ \text{(rapid rotation)}. \tag{6}$$

Similarly, the scalings for the convective velocity are:

$$u_{\rm conv} \sim u_\star\ \text{(slow rotation)},\quad \text{and}\quad u_{\rm conv} \sim u_\star\mathrm{Co}^{-1/6}\ \text{(rapid rotation)}. \tag{7}$$

Finally, the local Coriolis number $\mathrm{Co}_\ell = 2\Omega\ell_{\rm conv}/u_{\rm conv}$, can be shown to depend on $\mathrm{Ra_F^\star}$:

$$\mathrm{Co}_\ell \sim (\mathrm{Ra_F^\star})^{-1/3}\ \text{(slow rotation)},\quad \text{and}\quad \mathrm{Co}_\ell \sim (\mathrm{Ra_F^\star})^{-1/5}\ \text{(rapid rotation)}. \tag{8}$$

Here the convective length scale is estimated from the power spectrum of velocity, $E(k)$, for which $\boldsymbol{u}^2 = \int E(k)dk$, either by taking the wavenumber where the power has its maximum

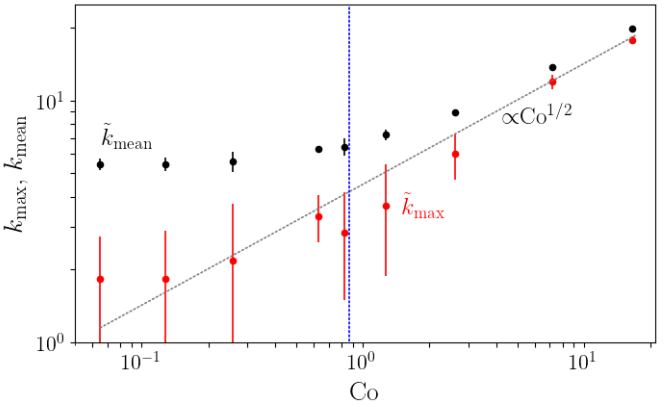

Figure 1. Mean ($k_{\rm mean}$) and peak ($k_{\rm max}$) wavenumbers from power spectra of velocity as a function of Co from simulations Set A from Käpylä (2023a). Data taken near the surface of the convectively unstable layer at $z/d = 0.85$. The dotted line shows the ${\rm Co}^{1/2}$ prediction from the CIA balance. The blue vertical dotted line indicates the solar value of ${\rm Co_F}$. The tildes indicate normalization by $k_{\rm H}$.

($k_{\rm max}$) or the mean wavenumber $k_{\rm mean} = \int kE(k)dk / \int E(k)dk$. The length scales $\ell_{\rm max}$ and $\ell_{\rm mean}$ are given by $\ell_{\rm max,mean} = L_{\rm x}/\tilde{k}_{\rm max,mean}$, where $\tilde{k}_{\rm max,mean} = k_{\rm max,mean}/k_{\rm H}$, and where $k_{\rm H} = 2\pi/L_{\rm x} = \pi/2d$ is the wavenumber corresponding to the horizontal extent of the simulation domain. Figure 1 shows $\tilde{k}_{\rm max}$ and $\tilde{k}_{\rm mean}$ from Set A. For slow rotation (${\rm Co} \lesssim 1$) both $\tilde{k}_{\rm max}$ and $\tilde{k}_{\rm mean}$ are approximately constant, although the former is already consistent with the ${\rm Co}^{1/2}$ scaling due to the large error estimates which are taken to be the standard deviation of the mean values calculated from several snapshots. For rapid rotation the ${\rm Co}^{1/2}$ scaling from the CIA balance is recovered for both $\tilde{k}_{\rm max}$ and $\tilde{k}_{\rm mean}$.

The case that the deep parts of the solar convection zone is strongly rotationally constrained has been discussed recently by Featherstone and Hindman (2016) and Vasil et al. (2021). Both of these studies argue that the maximum horizontal scale of convection is reduced by rotation in the deep parts of the convection zone, such that the largest convectively driven scale coincides with supergranules (20–30 Mm) at a spherical harmonic degree $\ell \approx 100$. Using Eq. (4) it is possible to compute ${\rm Co_F}$ at the base of the solar convection zone with $\Omega_\odot = 2.7 \cdot 10^{-6}$ s^{-1}, $H_{\rm p}^\odot \approx 5 \cdot 10^7$ m, $\rho^\odot \approx 200$ kg m^{-3}, and $F_{\rm tot}^\odot = L_\odot/(4\pi r_{\rm bot}^2)$, where $L_\odot = 3.83 \cdot 10^{26}$ W, and $r_{\rm bot} = 0.7R_\odot$, gives ${\rm Co_F^\odot} \approx 3.1$. On the other hand,

$$ {\rm Co} = \frac{u_\star}{u_{\rm rms}} \frac{{\rm Co_F}}{k_1 H_{\rm p}}. \tag{9} $$

For the current slowly rotating simulations in Sets A to C, $u_\star/u_{\rm rms} \approx 0.87$ (see, Figure 2), and $(k_1 H_{\rm p})^{-1} \approx 0.32$, such that the solar ${\rm Co_F}$ is achieved in a simulation with ${\rm Co} \approx 0.87$. Inspection of Figure 1 suggests that the Sun is somewhere in between the weakly rotationally influenced and the rotationally constrained regimes.

The dominant convective scale in a simulation with ${\rm Co} \approx 0.83$ and ${\rm Co_F} = 3.1$ is again estimated from the power spectrum of the velocity. In this case the maximum power occurs at wavenumber $\tilde{k}_{\rm max} = 3$ and the mean wavenumber is $\tilde{k}_{\rm mean} = 7$, corresponding to length scales $\ell_{\rm max} = 1.33d$ and $\ell_{\rm mean} = 0.57d$. The pressure scale height at the base of of the convective layer in this run is $H_{\rm p} = 0.49d$. Assuming the simulations to represent the deep parts of the convection zone at the interface to the radiative layer, the pressure scale height corresponds to $H_{\rm p}^\odot \approx 5 \cdot 10^7$ m. This leads to $\ell_{\rm max} \approx 135$ Mm and $\ell_{\rm mean} \approx 58$ Mm, respectively. These results seem to refute the idea that rotationally constrained convection can explain the supergranular scale as the largest convectively driven scale. Furthermore, Käpylä (2023a) showed that in the

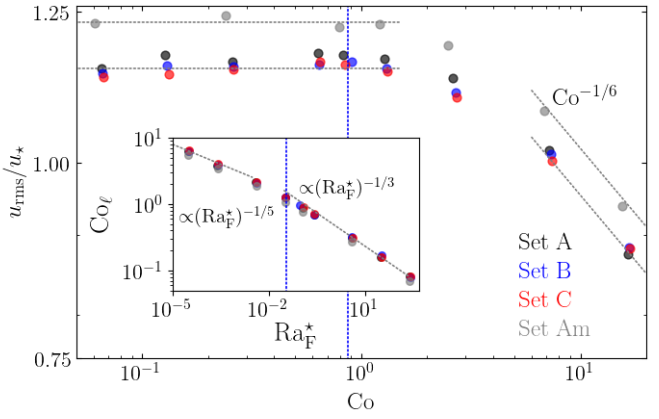

Figure 2. Volume-averaged rms-velocity as a function of Co from simulations in Sets A, B, C, and Am from Käpylä (2023a). The dotted lines are either constant (for $\mathrm{Co} \leq 1.5$) or proportional to $\mathrm{Co}^{-1/6}$ (for $\mathrm{Co} \geq 6$). The inset shows Co_ℓ as a function of $\mathrm{Ra}_\mathrm{F}^\star$ for the same runs with power laws proportional to $(\mathrm{Ra}_\mathrm{F}^\star)^{-1/5}$ for fast and $(\mathrm{Ra}_\mathrm{F}^\star)^{-1/3}$ for slow rotation corresponding to $\mathrm{Ra}_\mathrm{F}^\star \leq 3 \cdot 10^{-3}$ and $\mathrm{Ra}_\mathrm{F}^\star \geq 0.03$, respectively. The blue dotted vertical lines indicate the solar values of Co and $\mathrm{Ra}_\mathrm{F}^\star$, respectively.

simulations of Featherstone and Hindman (2016), where the supergranular scale is the dominant scale correspond to a value of Co_F that requires a rotation rate which is at least 15 times higher than in the Sun.

Figure 2 shows the time and volume-averaged rms-velocity from Sets A, B, C, and Am normalized by $u_\star$. The scalings for slow and rapid rotation from Eq. (7) are recovered for $\mathrm{Co} \lesssim 1.5$ and $\mathrm{Co} \gtrsim 6$, respectively. For Co exceeding the maximum values here ($\mathrm{Co} \approx 17$), the flow begins to develop a large-scale vortical component (see also Chan 2007; Käpylä et al. 2011) which is likely due to two-dimensionalization of turbulence, and extending the calculations to higher Co becomes challenging. Finally, the local Coriolis number Co_ℓ is shown in the inset of Figure 2. Co_ℓ adheres to the scalings given in Eq. (8) with respect to $\mathrm{Ra}_\mathrm{F}^\star$ for both slowly and rapidly rotating regimes.

4. Deardorff layer as a function of rotation

In the canonical models of stellar convection relying on mixing length theory (e.g. Böhm-Vitense 1958), the whole convection zone is unstably stratified and convection is thought to be driven locally by a superadiabatic temperature gradient

$$\Delta\nabla = \nabla - \nabla_\mathrm{ad} = -\frac{1}{H_\mathrm{p}}\frac{\mathrm{d}s}{\mathrm{d}z} > 0, \tag{10}$$

where $\nabla = \mathrm{d}\ln\overline{T}/\mathrm{d}\ln p$ is the logarithmic temperature gradient, $\nabla_\mathrm{ad} = (\mathrm{d}\ln\overline{T}/\mathrm{d}\ln p)_\mathrm{ad} = 1 - 1/\gamma$ is the corresponding adiabatic gradient, and where $\gamma = c_\mathrm{P}/c_\mathrm{V}$. If this were the case in the Sun, giant cell convection on the scale of 200 Mm is expected to be prominent. This is not observed in the Sun and 3D hydrodynamic simulations suggest that the deep parts of convective layers are often weakly subadiabatic (e.g. Roxburgh and Simmons 1993; Tremblay et al. 2015; Käpylä et al. 2017; Hotta 2017). This is thought to be due to the inherently non-local nature of convection which is driven by cooling near the surface instead of heating from the base as has been shown, e.g., in Käpylä et al. (2017).

This subadiabatic but convecting layer is referred to as the Deardorff zone (DZ), and it is characterised by $\Delta\nabla < 0$ and $\overline{F}_\mathrm{conv} > 0$, where

$$\overline{F}_\mathrm{conv} = \overline{F}_\mathrm{enth} + \overline{F}_\mathrm{kin} = c_\mathrm{P}\overline{(\rho u_z)'T'} + \tfrac{1}{2}\overline{\rho \boldsymbol{u}^2 u_z}, \tag{11}$$

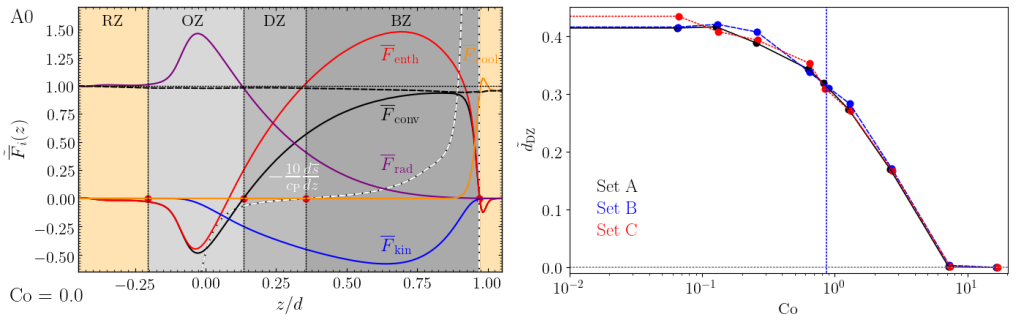

Figure 3. Left panel: Horizontally averaged energy fluxes from the non-rotating Run A0 from Käpylä (2023a). Grey (orange) areas indicate mixed (radiative) layers, and the red circles highlight the boundaries between the layers. The various zones are characterised as $\overline{F}_{\rm rad} \approx F_{\rm tot}$ (radiative; RZ), $\overline{F}_{\rm conv} < 0$, $\overline{F}_{\rm rad} > F_{\rm tot}$ (overshoot; OZ), $\overline{F}_{\rm conv} > 0$, $\Delta\nabla < 0$ (Deardorff; DZ), and $\overline{F}_{\rm conv} > 0$, $\Delta\nabla > 0$ (buoyancy; BZ). Right: Depth of the Deardorff layer ($d_{\rm DZ}$) as a function of Co from simulations in Sets A (black solid line), B (blue dashed), and C (red dotted). The blue dotted vertical line indicates the value of Co corresponding to the solar $\mathrm{Co_F}$. Adapted from Käpylä (2023a).

is the total convected flux (e.g. Cattaneo et al. 1991), which is the sum of the time and horizontal averages of the enthalpy and kinetic energy fluxes, and where the primes denote deviations from the horizontal average. The left panel of Figure 3 shows the flux balance from a non-rotating Run A0 from Käpylä (2023a), where in addition to $\overline{F}_{\rm conv}$, $\overline{F}_{\rm enth}$, and $\overline{F}_{\rm kin}$, also the radiative ($\overline{F}_{\rm rad} = -\overline{K}\mathrm{d}\overline{T}/\mathrm{d}z$) and cooling ($\overline{F}_{\rm cool} = -\int \overline{\mathscr{C}}\mathrm{d}z$) fluxes, as well as a quantity proportional to $\Delta\nabla$ are shown for reference. The DZ in this run is over 40 per cent of the pressure scale height at the base of the convection zone which is here defined as the lower boundary of the DZ. For the run closest to the solar value of $\mathrm{Co_F}$, $d_{\rm DZ} \approx 0.3H_{\rm p}$ which corresponds to 15 Mm in the Sun.

Figure 3 shows $d_{\rm DZ}$ as a fraction of the pressure scale height at the base of the convection zone as a function of rotation for Sets A, B, and C from Käpylä (2023a). The sets differ from each other in that the input energy flux is varied such that between the extreme cases (Sets A and C), $\mathscr{F}_{\rm n}$ decreases by factor of five. This has implications for the Mach number and also for the overshooting below the convection zone (e.g. Käpylä 2019). However, the depth of the DZ is virtually unaffected by the change of $\mathscr{F}_{\rm n}$. This is because the cooling time at the surface is varied inversely proportional to $\mathscr{F}_{\rm n}$ such that the thermal forcing remains unaffected.

5. Effects of surface forcing

There are some a few into the effects of varying surface forcing using convection simulations. For example, Cossette and Rast (2016) varied the superadiabatic gradient at the surface and found that it had a substantial effect on the convective length scale and deep convection zone dynamics. On the other hand, Hotta et al. (2019) found only a weak influence of the surface in a simulation that encompassed nominally the entire convection zone of the Sun.

Here a similar approach as in Cossette and Rast (2016) is explored with a simulation set-up that was used in Käpylä et al. (2017). In distinction to the simulations discussed above, the upper cooling layer is replaced by an imposed entropy gradient at the upper boundary, and the z-coordinate runs between $-0.5 \le z/d \le 1$ such that the transition between the initially isentropic and radiative layers is at $z = 0$. Furthermore, the SGS diffusion term has an extra term proportional to the mean entropy gradient:

$$\boldsymbol{F}_{\rm SGS} = -(\chi_{\rm SGS}\rho T\boldsymbol{\nabla}s' + \chi^{\rm m}_{\rm SGS}\rho T\boldsymbol{\nabla}\bar{s}), \tag{12}$$

where $\chi^{\rm m}_{\rm SGS}$ is non-zero only above $z/d = 0.95$, such that the second term on the rhs of Eq. (12) transports the heat flux through the upper boundary. Here $\mathrm{Pr_{SGS}} = 1$ and $\mathrm{Pr^m_{SGS}} = \nu/\chi^{\rm m}_{\rm SGS} =$

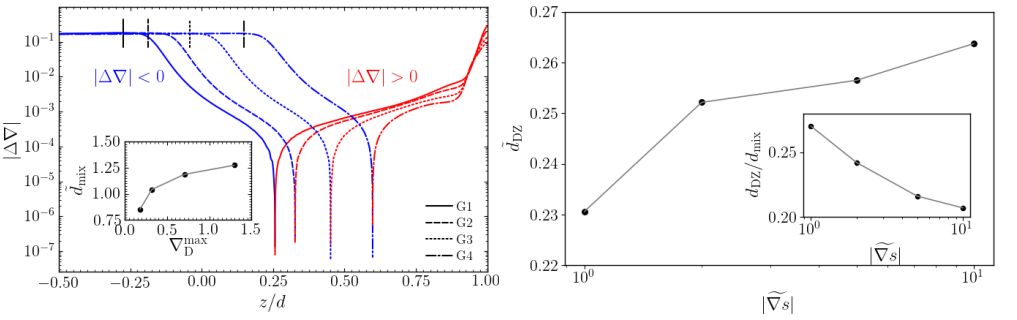

Figure 4. Left panel: Absolute value of the superadiabatic temperature gradient $\Delta\nabla$ for Runs G[1-4]. Red (blue) parts of the curves indicate regions where $\Delta\nabla > 0$ ($\Delta\nabla < 0$). The black vertical lines denote the bottom of the convectively mixed layer. The inset shows the depth of the mixed zone $\tilde{d}_{\rm mix} = d_{\rm mix}/d$ as a function $\nabla_{\rm D}^{\rm max}$. Right: depth of the Deardorff zone, $\tilde{d}_{\rm DZ} = d_{\rm DZ}/d$ as a function of $|\widetilde{\nabla s}|$. The inset shows the relative fraction of the Deardorff zone of the mixed zone as a function of $|\widetilde{\nabla s}|$.

0.5. In Käpylä et al. (2017), the entropy gradient at the surface was fixed to $\widetilde{\nabla s} = (d/c_{\rm P})(\boldsymbol{e}_z \cdot \boldsymbol{\nabla}\overline{s}) = -10$. Here four values between -1 and -10 for $\widetilde{\nabla s}$ are explored in Set G. In distinction to Cossette and Rast (2016) where a spatially fixed Newtonian cooling term was used which does not allow the depth of the convection zone to change appreciably, the current simulations use Kramers opacity law which enables this.

In the absence of convection the hydrostatic solution with the Kramers opacity law is convectively unstable only in a shallow surface layer (e.g. Barekat and Brandenburg 2014; Käpylä 2023a). This solution is modified by the onset of convection and the final outcome is expected to be sensitive to the surface physics. Decreasing $|\widetilde{\nabla s}|$ leads to a shallower convection zone as can be seen from the left panel of Figure 4. Furthermore, $\Delta\nabla$ near the surface decreases and the surface temperature increases. In the updated mixing length model of Brandenburg (2016), the enthalpy flux was quantified in terms of gradient ($\overline{F}_{\rm G}$) and non-gradient ($\overline{F}_{\rm D}$) contributions

$$\overline{F}_{\rm enth} = \overline{F}_{\rm G} + \overline{F}_{\rm D} = -\tau\overline{\rho}\,\overline{T}\left(\tfrac{1}{3}u_{\rm rms}^2\nabla_z\overline{s} + \overline{s'^2}g/c_{\rm P}\right) = \tfrac{1}{3}\overline{\rho}c_{\rm P}\overline{T}(\tau u_{\rm rms}^2/H_{\rm p})(\Delta\nabla + \nabla_{\rm D}), \quad (13)$$

where τ is a relaxation time, and where the magnitude of the non-gradient is characterised by

$$\nabla_{\rm D} = (3/\gamma)(\overline{s'^2}/c_{\rm P}^2){\rm Ma}^{-2}. \quad (14)$$

Brandenburg (2016) argued that $\nabla_{\rm D}$ in deeper parts is proportional to its maximum value near the surface, $\nabla_{\rm D}^{\rm max}$. The depth of the mixed layer $d_{\rm mix}$, consisting of the buoyancy, Deardorff, and overshoot zones, is shown as a function of $\nabla_{\rm D}^{\rm max}$ in the inset of the left panel of Figure 4 for the runs in Set G. While $d_{\rm mix}$ increases monotonically with $\nabla_{\rm D}^{\rm max}$ (corresponding to increasing $|\widetilde{\nabla s}|$), there appears to be no straightforward relation between the two. The depth of the Deardorff zone is not very sensitive to $|\widetilde{\nabla s}|$, although its size relative to the mixed zone decreases somewhat as $|\widetilde{\nabla s}|$ increases; see the inset of the right panel of Figure 4.

6. Conclusions

Several ways to address the "convective conundrum," or the discrepancy between convective velocity amplitudes in simulations and solar observations, were reviewed based on results from recent hydrodynamic Cartesian convection simulations. First the effects of rotation from Käpylä (2023a) were considered. These results suggest that the convective scale in the deep convection zone of the Sun is not sufficiently affected by rotation to reduce the largest convectively driven scale to the supergranular scale of 20-30 Mm as has been conjectured earlier (Featherstone and Hindman 2016; Vasil et al. 2021). These simulations also suggest that the

depth of the convective but formally stably stratified Deardorff zone is reduced as rotation increases, but that a substantial subadiabatic layer of about 15 Mm is still expected to be found at the base of the solar convection zone. Scaling laws of several dynamical quantities such as convective scale, velocity amplitude, and local Coriolis number were shown to follow scalings derived under the CIA balance (e.g. Stevenson 1979; Barker et al. 2014; Aurnou et al. 2020).

The effects of surface forcing were explored with a set of new simulations where the entropy gradient at the surface was imposed similarly as in Käpylä et al. (2017). Unlike in the previous studies in the literature that study the effects of the surface for the deep convection zone, the current simulations allow the depth of the convective layer to vary self-consistently. These preliminary results show that stronger surface forcing, in terms of a steeper entropy gradient, leads to a deeper convectively mixed layer. Although there is a monotonic dependence between the imposed entropy gradient and the depth of the convective layer, no clear relation between the two can be identified. However, the fraction of the Deardorff layer of the total depth of the convectively mixed layer decreases somewhat when the surface forcing is increased.

The results quoted above come with the caveat that the surface forcing of convection in the current simulations is assumed to be accurately modelled. This, however, cannot be guaranteed, and it is likely that much smaller scales need to be resolved to capture the effects of radiative cooling in the photosphere accurately (e.g. Kupka and Muthsam 2017). Furthermore, the effects of astrophysically relevant low Prandtl numbers (e.g. Spiegel 1962; Käpylä 2021) and vigorous magnetism (e.g. Hotta et al. 2022) are also likely to play important roles for solar and stellar convection.

Acknowledgements: The simulations were performed using the resources granted by the Gauss Center for Supercomputing for the Large-Scale computing project "Cracking the Convective Conundrum" in the Leibniz Supercomputing Centre's SuperMUC-NG supercomputer in Garching, Germany. This work was supported in part by the Deutsche Forschungsgemeinschaft (DFG, German Research Foundation) Heisenberg programme (grant No. KA 4825/4-1) and by the Munich Institute for Astro-, Particle and BioPhysics (MIAPbP) which is funded by the DFG under Germany´s Excellence Strategy – EXC-2094 – 390783311.

References

Aurnou, J. M., Horn, S., & Julien, K. 2020, Connections between nonrotating, slowly rotating, and rapidly rotating turbulent convection transport scalings. *Physical Review Research*, 2(4), 043115.

Barekat, A. & Brandenburg, A. 2014, Near-polytropic stellar simulations with a radiative surface. *A&A*, 571, A68.

Barker, A. J., Dempsey, A. M., & Lithwick, Y. 2014, Theory and Simulations of Rotating Convection. *ApJ*, 791(1), 13.

Böhm-Vitense, E. 1958, Über die Wasserstoffkonvektionszone in Sternen verschiedener Effektivtemperaturen und Leuchtkräfte. Mit 5 Textabbildungen. *ZAp*, 46, 108.

Brandenburg, A. 2016, Stellar mixing length theory with entropy rain. *ApJ*, 832, 6.

Brown, B. P., Miesch, M. S., Browning, M. K., Brun, A. S., & Toomre, J. 2011, Magnetic Cycles in a Convective Dynamo Simulation of a Young Solar-type Star. *ApJ*, 731, 69.

Brun, A. S., Miesch, M. S., & Toomre, J. 2004, Global-Scale Turbulent Convection and Magnetic Dynamo Action in the Solar Envelope. *ApJ*, 614, 1073–1098.

Cattaneo, F., Brummell, N. H., Toomre, J., Malagoli, A., & Hurlburt, N. E. 1991, Turbulent compressible convection. *ApJ*, 370, 282–294.

Chan, K. L. 2007, Rotating convection in f-boxes: Faster rotation. *Astron. Nachr.*, 328, 1059.

Christensen, U. R. 2002, Zonal flow driven by strongly supercritical convection in rotating spherical shells. *Journal of Fluid Mechanics*, 470(1), 115–133.

Cossette, J.-F. & Rast, M. P. 2016, Supergranulation as the Largest Buoyantly Driven Convective Scale of the Sun. *ApJ*, 829, L17.

Deardorff, J. W. 1961, On the Direction and Divergence of the Small-Scale Turbulent Heat Flux. *J. Atmosph. Sci.*, 18, 540–548.

Deardorff, J. W. 1966, The Counter-Gradient Heat Flux in the Lower Atmosphere and in the Laboratory. *J. Atmosph. Sci.*, 23, 503–506.

Fan, Y. & Fang, F. 2014, A Simulation of Convective Dynamo in the Solar Convective Envelope: Maintenance of the Solar-like Differential Rotation and Emerging Flux. *ApJ*, 789, 35.

Featherstone, N. A. & Hindman, B. W. 2016, The Emergence of Solar Supergranulation as a Natural Consequence of Rotationally Constrained Interior Convection. *ApJ*, 830, L15.

Gastine, T., Yadav, R. K., Morin, J., Reiners, A., & Wicht, J. 2014, From solar-like to antisolar differential rotation in cool stars. *MNRAS*, 438, L76–L80.

Ghizaru, M., Charbonneau, P., & Smolarkiewicz, P. K. 2010, Magnetic Cycles in Global Large-eddy Simulations of Solar Convection. *ApJ*, 715, L133–L137.

Gilman, P. A. 1977, Nonlinear Dynamics of Boussinesq Convection in a Deep Rotating Spherical Shell. I. *Geophys. Astrophys. Fluid Dynam.*, 8, 93–135.

Gilman, P. A. 1983, Dynamically consistent nonlinear dynamos driven by convection in a rotating spherical shell. II - Dynamos with cycles and strong feedbacks. *ApJS*, 53, 243–268.

Glatzmaier, G. A. 1985, Numerical simulations of stellar convective dynamos. II - Field propagation in the convection zone. *ApJ*, 291, 300–307.

Greer, B. J., Hindman, B. W., Featherstone, N. A., & Toomre, J. 2015, Helioseismic Imaging of Fast Convective Flows throughout the Near-surface Shear Layer. *ApJ*, 803, L17.

Hanasoge, S. M., Duvall, Thomas L., J., & DeRosa, M. L. 2010, Seismic Constraints on Interior Solar Convection. *ApJ*, 712(1), L98–L102.

Hanasoge, S. M., Duvall, T. L., & Sreenivasan, K. R. 2012, Anomalously weak solar convection. *Proc. Natl. Acad. Sci.*, 109, 11928–11932.

Hotta, H. 2017, Solar Overshoot Region and Small-scale Dynamo with Realistic Energy Flux. *ApJ*, 843, 52.

Hotta, H., Iijima, H., & Kusano, K. 2019, Weak influence of near-surface layer on solar deep convection zone revealed by comprehensive simulation from base to surface. *Science Advances*, 5(1), 2307.

Hotta, H., Kusano, K., & Shimada, R. 2022, Generation of Solar-like Differential Rotation. *ApJ*, 933(2), 199.

Käpylä, P. J. 2019, Overshooting in simulations of compressible convection. *A&A*, 631, A122.

Käpylä, P. J. 2021, Prandtl number dependence of stellar convection: Flow statistics and convective energy transport. *A&A*, 655, A78.

Käpylä, P. J. 2023,a Convective scale and subadiabatic layers in simulations of rotating compressible convection. *arXiv e-prints*,, arXiv:2310.12855.

Käpylä, P. J. 2023,b Transition from anti-solar to solar-like differential rotation: Dependence on Prandtl number. *A&A*, 669b, A98.

Käpylä, P. J., Browning, M. K., Brun, A. S., Guerrero, G., & Warnecke, J. 2023, Simulations of Solar and Stellar Dynamos and Their Theoretical Interpretation. *Space Sci. Rev.*, 219(7), 58.

Käpylä, P. J., Gent, F. A., Olspert, N., Käpylä, M. J., & Brandenburg, A. 2020, Sensitivity to luminosity, centrifugal force, and boundary conditions in spherical shell convection. *Geophysical and Astrophysical Fluid Dynamics*, 114(1-2), 8–34.

Käpylä, P. J., Käpylä, M. J., & Brandenburg, A. 2014, Confirmation of bistable stellar differential rotation profiles. *A&A*, 570, A43.

Käpylä, P. J., Mantere, M. J., & Brandenburg, A. 2012, Cyclic Magnetic Activity due to Turbulent Convection in Spherical Wedge Geometry. *ApJ*, 755, L22.

Käpylä, P. J., Mantere, M. J., & Hackman, T. 2011, Starspots due to Large-scale Vortices in Rotating Turbulent Convection. *ApJ*, 742, 34.

Käpylä, P. J., Rheinhardt, M., Brandenburg, A., Arlt, R., Käpylä, M. J., Lagg, A., Olspert, N., & Warnecke, J. 2017, Extended Subadiabatic Layer in Simulations of Overshooting Convection. *ApJ*, 845, L23.

Kupka, F. & Muthsam, H. J. 2017, Modelling of stellar convection. *Liv. Rev. Comp. Astrophys.*, 3, 1.

O'Mara, B., Miesch, M. S., Featherstone, N. A., & Augustson, K. C. 2016, Velocity amplitudes in global convection simulations: The role of the Prandtl number and near-surface driving. *Adv. Space Res.*, 58, 1475–1489.

Pencil Code Collaboration, Brandenburg, A., Johansen, A., Bourdin, P., Dobler, W., Lyra, W., Rheinhardt, M., Bingert, S., Haugen, N., Mee, A., Gent, F., Babkovskaia, N., Yang, C.-C., Heinemann, T., Dintrans, B., Mitra, D., Candelaresi, S., Warnecke, J., Käpylä, P., Schreiber, A., Chatterjee, P., Käpylä, M., Li, X.-Y., Krüger, J., Aarnes, J., Sarson, G., Oishi, J., Schober, J., Plasson, R., Sandin, C., Karchniwy, E., Rodrigues, L., Hubbard, A., Guerrero, G., Snodin, A., Losada, I., Pekkilä, J., & Qian, C. 2021, The Pencil Code, a modular MPI code for partial differential equations and particles: multipurpose and multiuser-maintained. *The Journal of Open Source Software*, 6(58), 2807.

Proxauf, B. 2021,. *Observations of large-scale solar flows*. PhD thesis, Georg August University of Göttingen, Germany.

Roxburgh, L. W. & Simmons, J. 1993, Numerical studies of convective penetration in plane parallel layers and the integral constraint. *A&A*, 277, 93.

Spiegel, E. A. 1962, Thermal Turbulence at Very Small Prandtl Number. *J. Geophys. Res.*, 67(3), 3063.

Spruit, H. 1997, Convection in stellar envelopes: a changing paradigm. *Mem. Soc. Astron. Italiana*, 68, 397.

Stein, R. F. & Nordlund, A. 1989, Topology of convection beneath the solar surface. *ApJ*, 342, L95–L98.

Stevenson, D. J. 1979, Turbulent thermal convection in the presence of rotation and a magnetic field: A heuristic theory. *Geophysical and Astrophysical Fluid Dynamics*, 12(1), 139–169.

Thompson, M. J., Christensen-Dalsgaard, J., Miesch, M. S., & Toomre, J. 2003, The Internal Rotation of the Sun. *ARA&A*, 41, 599–643.

Tremblay, P.-E., Ludwig, H.-G., Freytag, B., Fontaine, G., Steffen, M., & Brassard, P. 2015, Calibration of the Mixing-length Theory for Convective White Dwarf Envelopes. *ApJ*, 799, 142.

Vasil, G. M., Julien, K., & Featherstone, N. A. 2021, Rotation suppresses giant-scale solar convection. *Proceedings of the National Academy of Science*, 118(31), e2022518118.